Development of Graphene Oxide Nanofluids From Recycled Graphite: Part I-Materials Characterization

Mourad Makhlouf, Zoubir Benmaamar, Didier Villemin, Tahar Tayebi

Development of Graphene Oxide Nanofluids From Recycled Graphite: Part I—Materials Characterization

Mourad Makhlouf[1,*], Zoubir Benmaamar[2], Didier Villemin[3], and Tahar Tayebi[4]

[1]*Laboratory of Research in Combustion, Detonation and Ballistics-M A C-D P HB, Tipaza, 9000, Algeria*
[2]*Laboratory of Energy Processes and Nanotechnology EPNL, University of Blida, 9000, Algeria*
[3]*Molecular and Thio-Organic Chemistry Laboratory MTCL .ENSICAEN6 Boulevard Maréchal Juin, 14050 Caen, France*
[4]*Mechanical Engineering Department, Faculty of Sciences and Technology, University Mohamed El Bachir El Ibrahimi of Bordj Bou Arreridj, El-Anasser, 34030, Algeria*

This work explores the synthesis of graphene oxide (GO) nanoflakes from recycled graphite using a modified Hummers method. The effectiveness of this approach was evaluated through comprehensive characterization techniques. Scanning electron microscopy (SEM) revealed the formation of uniform GO with stacked, flat sheets. X-ray diffraction (XRD) confirmed the presence of oxygen-containing functional groups on the GO surface by identifying a characteristic peak. Fourier transform infrared (FT-IR) spectroscopy successfully identified key functional groups (carboxyl, aromatic C═C, alkoxy, and hydroxyl) responsible for the unique properties of GO. Raman spectroscopy analysis confirmed the presence of graphene with a less distorted structure through characteristic D and G bands. However, the ID/IG ratio was not a reliable measure of interdefect distance due to the high defect density in GO. Brunauer-Emmett-Teller (BET) and BJH analysis classified the OG as a mesoporous material with a significant surface area. Thermogravimetric analysis (TGA) verified the thermal stability of GO, revealing two distinct mass losses: one due to adsorbed water elimination and another due to the decomposition of oxygenated functional groups.

KEYWORDS: Nanofluid, Nanomaterial, Recycled Graphite, Graphene Oxide, Hummer's Method.

1. INTRODUCTION

Nanoscale materials are incorporated into working fluids, resulting in stable suspensions known as "nanofluids".[1] Nanofluids find application in various fields where they enhance the efficiency of systems and processes by improving thermal properties and heat transfer capabilities. Extensive research has delved into the manufacturing methods, fundamental attributes, heat transfer performance, transport behavior, and practical utilization of nanofluids to enhance overall efficiency.

Studies examining the fundamental characteristics of nanofluids have predominantly focused on parameters such as thermal conductivity, density, viscosity, specific heat, and suspension stability.[2,3] Investigations into the heat transfer performance of nanofluids have primarily centered on aspects like heat transfer efficiency, pressure drop, and energy consumption within single tubes[4,5] or heat exchangers with varying geometries.[6]

Currently, nanofluids find application in diverse systems, including vehicle cooling systems, heat recovery processes, refrigeration and air conditioning systems, and solar collectors.[7,8]

Due to their exceptional foundational properties, nanofluids serve as enhancers for system performance and equipment efficiency. However, it's crucial to take into account the long-term stability of nanofluid suspensions and their cost-effectiveness. These factors are contingent upon the techniques used for manufacturing nanofluids. Broadly speaking, the synthesis of nanofluids can be categorized into one-step synthesis methods and two-step synthesis methods.

One-step synthesis methods involve the direct fabrication of nanoparticles within the base liquid, resulting in the formation of nanofluids. These one-step synthesis techniques typically include the sputtering method,[9,10] arc discharge method,[11–13] laser ablation method,[14,15] water-assisted synthesis method,[16] and chemical reaction-generated method.[17] One-step synthesis

*Author to whom correspondence should be addressed.
Email: makhlouf.amia@gmail.com

processes generally possess inherent mechanisms for regulating particle size: larger particles tend to settle at the container's bottom, while ultra-fine particles remain suspended in the liquid. Achieving nanofluids with exceptional suspension properties often involves eliminating the precipitated particles or using a centrifuge to control the size of suspended particles. Consequently, a minimal amount of dispersant or surfactant is required to enhance the suspension characteristics of nanofluids produced through one-step synthesis methods. Nonetheless, a drawback of these methods lies in the fact that the preparation and process conditions can influence the size, shape, and concentration of nanoparticles, leading to a wide range of particle sizes and challenges in concentration control.

In two-step synthesis approaches, nanoparticles are initially generated and then dispersed within a base liquid to create nanofluids. The dispersion processes commonly employed in two-step synthesis encompass mechanical agitation techniques, such as magnetic stirring, homogenization, and mixing,[8,18] ultrasonic dispersion methods utilizing equipment like ultrasonic baths, ultrasonic processors, and ultrasonic disruptors,[19,20] as well as grinding processes.[21] Additionally, enhancing nanofluid suspension performance and ensuring long-term stability can be achieved by introducing stabilizers, like dispersants or surfactants,[19,21] or by adjusting the pH value.[22,23]

Generally, two-step synthesis methods offer a simpler alternative to one-step synthesis techniques. This is because nanoparticles can either be produced in-house or procured and subsequently added to a base liquid to generate nanofluids. Two-step synthesis methods offer several advantages over one-step methods, including the ease and speed of preparing large quantities of nanofluids, better control over nanoparticle concentration, and a narrower particle size distribution. However, there is a propensity for nanoparticle agglomeration during the addition process, which can lead to suboptimal suspension quality. Therefore, two-step synthesis often necessitates the use of dispersion equipment or the incorporation of stabilizers (surfactants or dispersants) to counteract nanoparticle agglomeration, ensure dispersion, and maintain long-term suspension stability.

In this study, we used Hummer's method for the fabrication of graphene oxide GO. To validate the viability of this approach, we performed a comprehensive characterization of GO using appropriate instrumentation and testing protocols. This included an assessment of their morphology, structure, particle size and other fundamental properties.

2. EXPERIMENT AND METHODS

2.1. Chemicals and Materials

Graphite from drilling mold. $NaNO_3$, H_2SO_4, $KMnO_4$, H_2O_2, HCl chemicals were purchased from Sigma Aldrich. distilled water.

2.2. Synthesis of Graphene Oxide (GO)

Graphene oxide was synthesized using the Hummers method by oxidizing graphite.[24]

First, 2 g of graphite flakes and 2.5 g of $NaNO_3$ were mixed in 108 mL of concentrated sulfuric acid (H_2SO_4) in a 1000 mL volumetric flask. The flask was kept in an ice bath (0–5 °C) and stirred continuously for 2 hours. Then, 15 g of potassium permanganate was added to the suspension very slowly, carefully controlling the rate of addition to keep the reaction temperature below 15 °C. The ice bath was then removed, and the mixture was stirred at 35 °C until it became a pasty brownish color. The mixture was then stirred for an additional 2 days. Next, 100 mL of water was slowly added to the mixture, rapidly increasing the reaction temperature to 98 °C with effervescence and changing the color to brown. An additional 200 mL of water was then added, and the solution was stirred continuously. Finally, 15 mL of hydrogen peroxide (H_2O_2) was added to terminate the reaction, as evidenced by the appearance of a yellow color.

To purify the graphene oxide, the mixture was washed by rinsing and centrifugation with 5% hydrochloric acid (HCl) and then deionized (DI) water several times. After filtration and drying under vacuum at room temperature, the graphene oxide (GO) was obtained as a powder.

2.3. Characterization

The morphology of the samples was investigated using scanning electron microscopy (SEM).

The chemical composition of the materials was determined by Fourier transform infrared spectroscopy (FT-IR). X-ray diffraction (XRD) analysis was employed to verify the crystallinity of the samples. Raman spectroscopy provided insights into the vibrational properties of the GO sheets. Brunauer–Emmett–Teller (BET) and BJH methods were used to determine the specific surface area of the material. Finally, thermogravimetric analysis (TGA) was conducted to assess the thermal stability and measure the mass loss behavior of the sample.

3. RESULTS AND DISCUSSION

Scanning electron microscopy (SEM) images of our graphene oxide samples are shown in Figure 1. The images reveal the unique structure of our graphene oxide, which is highly uniform at the nanoscale. Wide, flawless sheets of graphene oxide are stacked on top of each other. At higher magnification, folds and islands are observed in the graphene oxide sheets.

The morphology of a GO sheet refers to its shape, size, and structure. GO sheets are typically flat and two-dimensional, with a lateral size of 1–10 micrometers and a thickness of 1–2 nanometers. However, the morphology of GO sheets can vary depending on the synthesis method and the conditions used. The presence of functional groups on the surface of GO sheets can also affect

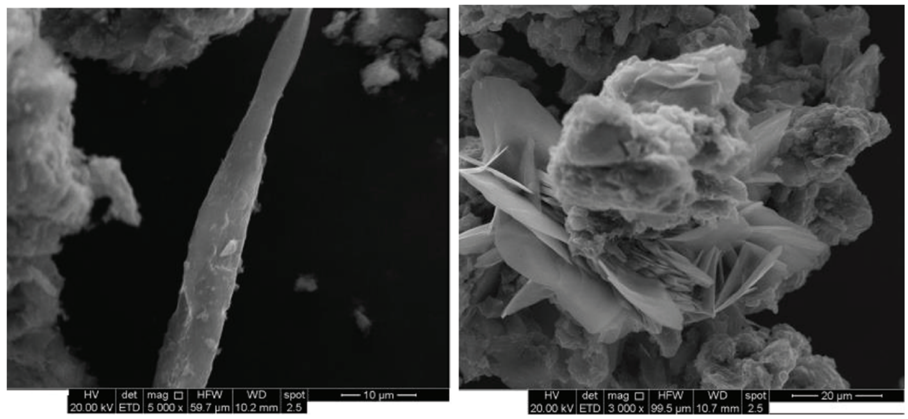

Fig. 1. SEM of GO sheet.

their morphology. GO sheets with a high concentration of oxygen-containing functional groups are more hydrophilic. X-ray diffraction (XRD) was performed to characterize the crystallographic structure of graphene oxide (GO) sheets. The XRD pattern (Fig. 2) shows a characteristic peak at $2\theta = 10.34°$, corresponding to a d-spacing of 8.546 Å. This is consistent with the interlayer spacing of GO sheets reported in the literature, which is due to the presence of oxygen-rich functional groups on both sides of the sheets and water molecules trapped between the sheets.

The X-ray diffraction (XRD) structure of graphene oxide (GO) is characterized by a single peak at a 2θ angle of around 10°. This peak corresponds to the interlayer spacing between the GO sheets, which is typically around 8.5 Å. The large interlayer spacing is due to the presence of oxygen-rich functional groups on the surface of the GO sheets, as well as water molecules trapped between the sheets. Fourier-transform infrared (FTIR) spectroscopy was used to characterize the functional groups of the graphene oxide (GO) sheets, as shown in Figure 3.

Fourier transform infrared (FT-IR) analysis of graphene oxide (GO) provides valuable information about the

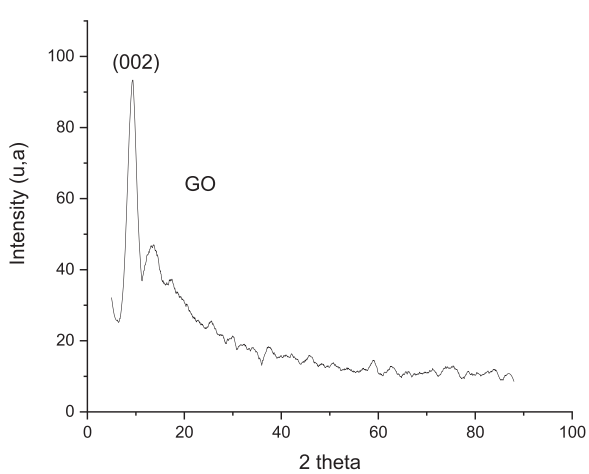

Fig. 2. The XRD of GO sheet.

structure and properties of the material. The absorption bands in the FT-IR spectrum correspond to specific vibrations of chemical bonds present in the material. The most important absorption bands in the FT-IR spectrum of GO are as follows 1700 cm^{1}: carboxyl C=O absorption band, which is an indicator of the presence of carboxyl groups (COOH). Carboxyl groups are responsible for the negative charge of GO, at 1584 cm^{1} aromatic C=C bond absorption band, which is an indicator of the presence of aromatic groups. 1038 cm^{1}: alkoxy C–O bond absorption band, which is an indicator of the presence of alkoxy groups (C–O–R). Alkoxy groups are also produced during the oxidation of graphene, at 3099 cm^{1}: hydroxyl –OH bond absorption band, which is an indicator of the presence of hydroxyl groups (–OH). Hydroxyl groups are produced during the oxidation of graphene. The presence of these absorption bands confirms the presence of the above-mentioned functional groups in GO. These functional groups give GO its unique properties, such as its negative charge, electrical conductivity, and water absorption capacity.[25,26] Raman spectroscopy of graphite and graphene oxide (GO) (Figs. 4 and 5) typically reveals two characteristic peaks: the D band at around 1350 cm^{-1}; and the G band at around 1574 cm^{-1}. The presence of both the D and G bands confirms the presence of graphene with a less distorted and more transparent structure. Additionally, an increase in the intensity of the D band relative to the G band indicates a significant decrease in the size of the sp^2 domains in the graphene plane due to the oxidation process and the formation of highly transparent graphene nanofilaments.

The ID/IG ratio, which has been established as a measure of the interdefect distance in graphene, is not reliable when applied to GO and rGO.[27,28] Ferrari and Robertson described an amorphization process in which the ID/IG ratio of carbon (sp^2) increases with the spread of defects, following the square of the crystallite size.[29] Thus, they define a transition between carbons with a crystallite size less than ~2 nm, which should follow the Ferrari-Robertson relationship, and those with larger crystallites,

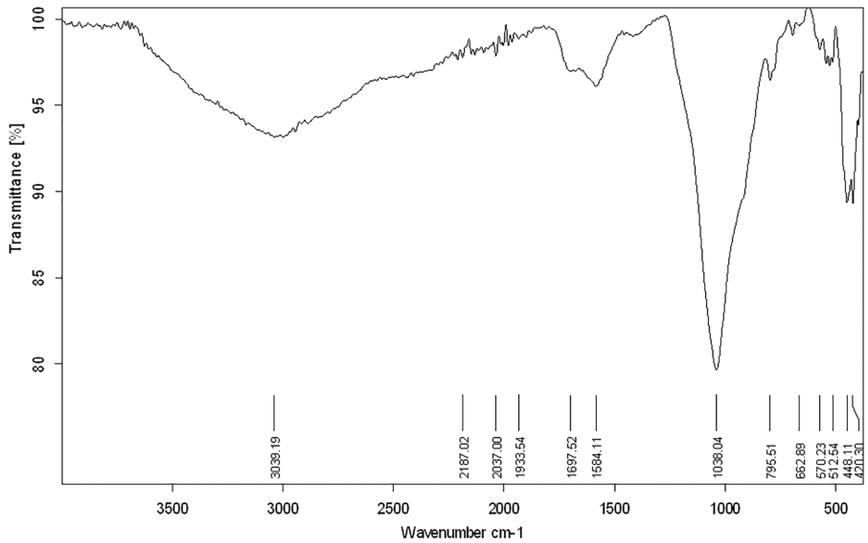

Fig. 3. The FT-IR patters of GO sheet.

which follow the Tuinstra-Koenig relationship. The discontinuity in the relationship to structure is attributed to the bending of aromaticity at extremely high defect densities.

Kurniasari et al. have shown that if the defect intensity ratio (ID/IG) increases, this implies an increase in the number of defects.[30]

The decrease in the ratio of the intensities of the D and G bands (ID/IG ratio) (Table I) and the shift of their position towards lower frequencies indicate a less extensive graphitic domain, attributed to an increase in the level of disorder of the sp^2 bonds, and an increase in the number of sp^3 bonds in the structure.[31]

The BET specific surface area of the OG was determined using the nitrogen (N_2) adsorptiondesorption isotherm shown in Figure 6. The isotherm of the OG, according to the classification of the International Union of Pure and Applied Chemistry (IUPAC), is of type IV. An increase in the adsorbed volume in the P/P0 range of 0.7–1 is attributed to capillary condensation accompanied by a hysteresis loop. The shape confirms that the material is a mesoporous material. The results of the specific surface area, pore volume, and pore diameter obtained by the BET and BJH methods are given in Table I.

The specific surface area of graphene, a crucial property for many applications, can vary significantly depending on the preparation method. Generally, it falls within a range of 200 to 2500 square meters per gram (m^2/g).[32]

Table I. Parameter results obtained by the BET and BJH methods.

Specific surface area (m^2/g)			Pore volume (cm^3/g)	Average pore diameter (nm)
S_{BET}	$S_{Langmuir}$	S_{BJH}		
624.96	1482.47	1581.62	1.901	48.05

Incomplete exfoliation and aggregation during synthesis are key factors influencing this value. Our results demonstrate that the S_{BET} surface area of the studied graphene oxide (OG) is 624.9633 m^2/g, while the $S_{Langmuir}$ surface area is 1482.47 m^2/g. interestingly, the BJH method yielded a higher surface area for the OG, at 1581.62 m^2/g. This difference can be attributed to the BJH method's sensitivity towards larger pores compared to BET and Langmuir techniques. The BJH method based on the adsorption and desorption isotherm, also allowed us to determine the pore volume of the OG as 1.901 cm^3/g and the average pore diameter as 48.05 angstroms (Å). Assessing the thermal behavior of graphene oxide (GO) is crucial for determining its thermal stability. Thermogravimetric analysis (TGA) is a widely used technique to investigate the thermal stability of materials.

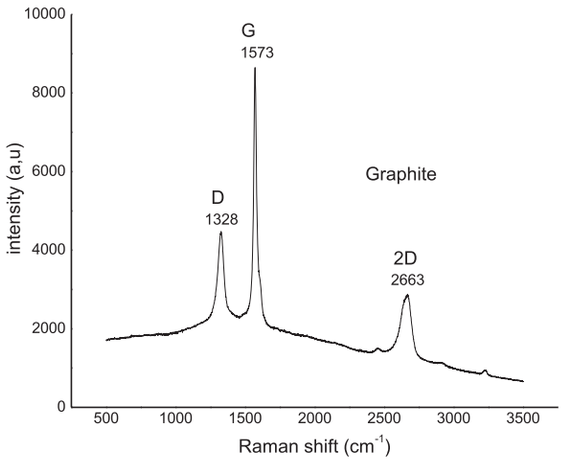

Fig. 4. Raman spectrum of graphite.

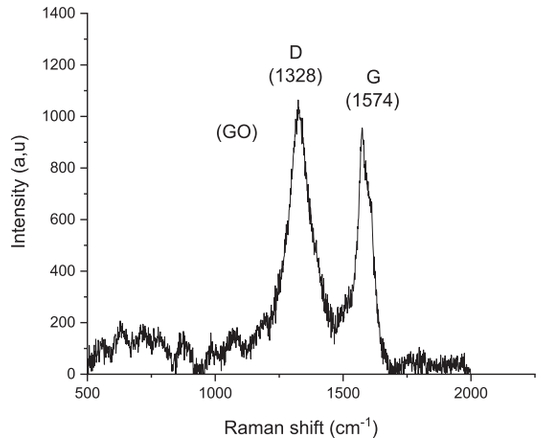

Fig. 5. Raman spectrum of GO.

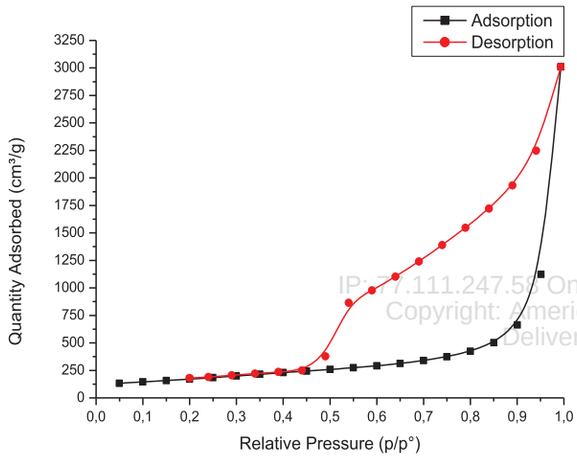

Fig. 6. OG sheet nitrogen adsorption/desorption isotherm.

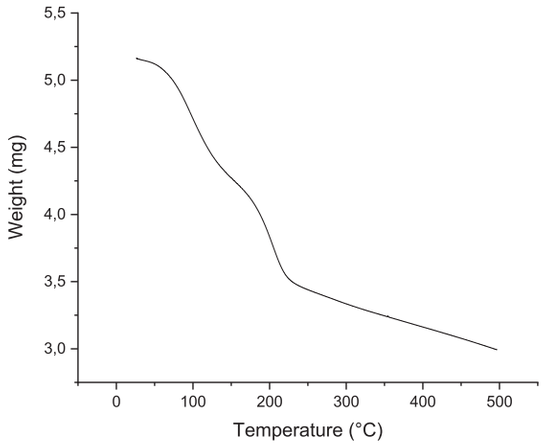

Fig. 7. TGA thermograms of GO.

Figure 7 presents the TGA thermograms of GO, illustrating the evolution of mass loss as a function of temperature. A first mass loss of 9% is observed at 98 °C. This loss is attributed to the elimination of adsorbed water on the surface and within the structure of GO. A second weight loss of 29% occurs at 208 °C. This significant mass loss is due to the decomposition of oxygenated functional groups present on the surface of GO. These functional groups, introduced during the graphite oxidation process, are typically hydroxyl groups (–OH), carboxylic groups (–COOH), and epoxy groups (–O–). Their decomposition releases gases such as CO_2 and H_2O, explaining the observed mass loss.

4. CONCLUSION

This study successfully synthesized graphene oxide (GO) nanoflakes from recycled graphite using a modified Hummers method. Various characterization techniques confirmed the successful preparation of GO with the desired properties. SEM images revealed a uniform structure of GO with wide, flat sheets stacked on top of each other. The XRD pattern confirmed the presence of oxygen-containing functional groups on the GO sheets, indicated by a characteristic peak at $2\theta = 10.34°$. FT-IR analysis identified the presence of functional groups like carboxyl (C═O), aromatic C═C, alkoxy (C–O), and hydroxyl (–OH) groups, responsible for the unique properties of GO. Raman spectra showed characteristic D and G bands, confirming the presence of graphene with a less distorted structure. However, the ID/IG ratio was not a reliable measure of inter-defect distance due to the high defect density in GO. The N2 adsorption–desorption isotherm classified the OG as a mesoporous material. The BET surface area of the OG was 624.9633 m^2/g, while the BJH method yielded a higher value of 1581.62 m^2/g due to its sensitivity towards larger pores. TGA confirmed the thermal stability of GO. Two distinct mass losses were observed: the first at 98 °C due to adsorbed water elimination and the second at 208 °C due to the decomposition of oxygenated functional groups. These results demonstrate the feasibility of synthesizing GO nanoflakes from recycled graphite using a modified Hummers method. The obtained GO possesses desirable properties like high surface area and functional groups, making it a promising candidate for various applications.

Conflicts of Interest

The authors declare that there is no conflict of interests regarding the publication of this paper.

References and Notes

1. S. U. S. Choi, Enhancing thermal conductivity of fluids with nanoparticles, in Developments and Applications of Non-Newtonian Flows, D. A. Siginer and H. P. Wang, eds., vol. 231, pp.99–105, ASME FED, **(1995)**.
2. K. S. Suganthi and K. S. Rajan, *Int. J. Heat Mass Transfer* 55, 7969 **(2012)**.
3. T. P. Teng, *Energy Convers. Manage.* 67, 369 **(2013)**.
4. L. Syam Sundar, M. T. Naik, K. V. Sharma, M. K. Singh, and T. C. Siva Reddy, *Exp. Therm Fluid Sci.* 37, 65 **(2012)**.

5. K. Wongcharee and S. Eiamsa-ard, *International Communications in Heat and Mass Transfer* 39, 251 **(2012)**.
6. C. J. Ho and W. C. Chen, *Appl. Therm. Eng.* 50, 516 **(2013)**.
7. O. Mahian, A. Kianifar, S. A. Kalogirou, I. Pop, and S. Wongwises, *Int. J. Heat Mass Transfer* 57, 582 **(2013)**.
8. J. Y. Jung, E. S. Kim, Y. Nam, and Y. T. Kang, *International Journal of Refrigeration* 36, 1056 **(2013)**.
9. Y. Hwang, J.-K. Lee, J.-K. Lee, Y.-M. Jeong, S.-I. Cheong, Y.-C. Ahn, and S. H. Kim, *Powder Technol.* 186, 145 **(2008)**.
10. E. Tamjid and B. H. Guenther, *Powder Technol.* 197, 49 **(2010)**.
11. C.-H. Lo, T.-T. Tsung, and L.-C. Chen, *J. Cryst. Growth* 277, 636 **(2005)**.
12. H. Chang and Y.-C. Chang, *J. Mater. Process. Technol.* 207, 193 **(2008)**.
13. G.-J. Lee, C. K. Kim, M. K. Lee, C. K. Rhee, S. Kim, and C. Kim, *Thermochim. Acta* 542, 24 **(2012)**.
14. F. Barreca, N. Acacia, E. Barletta, D. Spadaro, G. Currò, and F. Neri, *Appl. Surf. Sci.* 256, 6408 **(2010)**.
15. V. Thongpool, P. Asanithi, and P. Limsuwan, *Procedia Engineering* 32, 1054 **(2012)**.
16. M. Bansal, C. Lal, L. S. Tanwar, and V. Gupta, *Mater. Sci. Eng., B* 157, 93 **(2009)**.
17. G. Yang, Z. Zhang, S. Zhang, L. Yu, and P. Zhang, *Mater. Res. Bull.* 48, 1716 **(2013)**.
18. T.-P. Teng, Y.-H. Hung, T.-C. Teng, and J.-H. Chen, *Nanoscale Research Letters* 6, 1 **(2011)**.
19. A. Kosmala, Q. Zhang, R. Wright, and P. Kirby, *Mater. Chem. Phys.* 132, 788 **(2012)**.
20. M. Wan, R. R. Yadav, K. L. Yadav, and S. B. Yadaw, *Exp. Therm. Fluid Sci.* 41, 158 **(2012)**.
21. H. Hezaveh, A. Fazlali, and I. Noshadi, *Journal of the Taiwan Institute of Chemical Engineers* 43, 159 **(2012)**.
22. P. Selvakumar and S. Suresh, *Exp. Therm. Fluid Sci.* 40, 57 **(2012)**.
23. M. Naraki, S. M. Peyghambarzadeh, S. H. Hashemabadi, and Y. Vermahmoudi, *International Journal of Thermal Sciences* 66, 82 **(2013)**.
24. J. Chen, B. Yao, C. Li, and G. Shi, *Carbon N. Y.*, 64, 225 **(2013)**.
25. Y. Zhang and C. Pan, *Journal of Materials Science* 46, 2622 **(2011)**.
26. J. Shen, M. Shi, B. Yan, H. Ma, N. Li, and M. Ye, *Nano Research* 4, 795 **(2011)**.
27. G. P. Kotchey, *ACS Nano* 5, 2098 **(2011)**.
28. S. Stankovich, *Carbon* 7, 1558 **(2007)**.
29. A. Ferrari and C. Robertson, *J. Phys. Rev. B.* 61, 14095 **(2000)**.
30. Kurniasari, A. Maulana, A. Y. Nugraheni, D. N. Jayanti, S. Mustofa, M. A. Baqiya, and Darminto, *IOP Conf. Ser.: Mater. Sci. Eng.* 196, 012021 **(2017)**.
31. M. Lucchese, M. Stavale, F. Ferreira, E. Vilani, C. Moutinho, and R. Achete, *Carbon* 48, 1592 **(2010)**.
32. L. Yu, L. Wang, W. Xu, L. Chen, M. Fu, J. Wu, and D. Ye, *Journal of Environmental Sciences* 67, 171 **(2018)**.